J. Fluid Mech. (1987), *vol.* 175, *pp.* 343–362
Printed in Great Britain

The response of a compressible turbulent boundary layer to short regions of concave surface curvature

By MOHAN JAYARAM, MARGARET W. TAYLOR AND ALEXANDER J. SMITS

Gas Dynamics Laboratory, Department of Mechanical and Aerospace Engineering, Princeton University, Princeton, NJ 08544, USA

(Received 24 January 1986)

Experiments were performed to investigate the supersonic flow of a turbulent boundary layer over short regions of concave surface curvature. Upstream of each curved wall, the free-stream Mach number was 2.87, and the incoming boundary layer was typical of a two-dimensional, zero-pressure-gradient, high-Reynolds-number flow. Two different curvatures were used, with radii of curvature equal to 10 and 50 initial boundary-layer thicknesses (Models I and II, respectively). The turning angle was 8° in each case. As the boundary layer passed through the curved region, it experienced a strong adverse pressure gradient, as well as the destabilizing influences of bulk compression and concave curvature. Downstream of the curved walls, the flow relaxed on a short plane wall. The mean and turbulent field for each flow was investigated, using normal and inclined hot wires to measure the turbulent fluctuations. Wherever possible, the results were compared with those from a corresponding 8° ramp. The ramp and Model I exhibited a very similar behaviour: turbulence levels increased significantly, and there was a marked increase in structural parameters such as the stress ratio $-\overline{u'v'}/\overline{u'^2}$ and the length- and timescales of the turbulent motions. Model II behaved quite differently: although the turbulence levels increased, structural parameters were essentially unchanged. The similarities between the ramp and Model I results suggest that the perturbation in both cases is 'rapid' in that the perturbation can be described in terms of total strains rather than local strains. In contrast, the flow in Model II is sensitive to the local variations in the strain rate.

1. Introduction

In this investigation, we examine the behaviour of a supersonic turbulent boundary layer experiencing a short region of concave surface curvature. This investigation was prompted in part by recent studies of shock-wave/boundary layer interactions generated by two-dimensional compression corners (Settles, Fitzpatrick & Bogdonoff 1979; Smits & Muck 1987). In that work, extensive measurements were made to investigate the effect of shock strength on boundary-layer behaviour. The shock strength was varied at a constant Mach number of 2.87 by increasing the compression corner angle from 8° to 24°, and the corresponding flows ranged from a fully attached case to a case with a significant region of separated flow. The incoming boundary layer was identical in all cases. The interaction distorted the boundary-layer parameters considerably; in particular, the turbulent stresses were dramatically amplified. Four separate mechanisms for turbulence amplification were identified: 'direct' amplification by the shock wave; amplification by shock-wave oscillation; the destabilizing

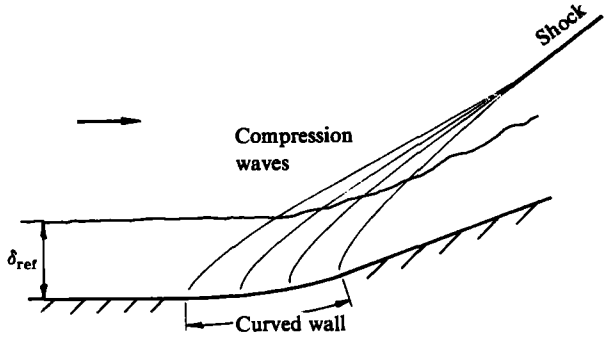

FIGURE 1. Boundary layer on a curved wall in supersonic flow.

effect of compression downstream of the shock, and the destabilizing effect of concave curvature.

The present study investigates the effect of perturbation rate on the boundary-layer behaviour. In the compression-corner experiment, the flow variables change discontinuously through the shock wave, and continue to change for a short distance downstream until the pressure rise is complete. Here, we spread the wall-pressure rise over several boundary-layer thicknesses by curving the wall. The perturbation rate can then be controlled by changing the radius of curvature while the overall perturbation level can be kept constant by maintaining the same turning angle. As the radius of curvature increases, the shock wave moves away from the wall until it takes up a position outside the boundary layer, where it no longer has any direct influence on the boundary-layer behaviour. The radius of curvature for both models investigated here is large enough for the shock to form outside the boundary layer. As the boundary-layer flow passes through the curved region, therefore, the pressure rises smoothly, and the layer is subjected simultaneously to the effects of an adverse pressure gradient, bulk compression and concave streamline curvature (see figure 1). Within the region of pressure rise, normal pressure gradients also act.

Bulk compression and concave curvature are examples of what Bradshaw (1973) called 'extra' strain rates, that is, strain rates additional to the main shear $\partial U/\partial y$. Other examples include streamline divergence and longitudinal pressure gradient. Interestingly, the underlying mechanisms appear to share many common features. For instance, curvature and buoyancy effects can be linked by an analogy which is quantitatively useful (Bradshaw 1974). More to the point, Green suggested that in a two-dimensional flow there may exist a strong analogy between divergence and compression; both reduce the cross-sectional area of a fluid element and amplify the spanwise vorticity component by conservation of angular momentum (see Bradshaw 1973).

The effects of concave curvature, acting in the absence of other extra strain rates, are reasonably well known. In subsonic flows, the turbulence levels are amplified strongly, the turbulence lengthscales increase, and longitudinal roll-cells are formed through a Taylor–Goertler-like instability. Prolonged application of mild curvature appears qualitatively to have similar effects to short regions of high curvature (see, for instance, So & Mellor 1972; Ramaprian & Shrivaprasad 1978; Smits, Eaton & Bradshaw 1979; Muck 1982). In supersonic flows, similar effects appear to occur. For example, Thomann (1968) obtained heat transfer data for a zero pressure gradient, Mach 2.5 turbulent boundary layer on a concavely curved wall and found that even weak curvature dramatically increased the heat transfer rates.

Re_{ref}/m	6.3×10^7/m
M_{ref}	2.87
p_0	6.9×10^5 N/m^2
p_w	2.3×10^4 N/m^2
T_w/T_0	1.04
T_0	270 K
U_{ref}	572 m/s
δ_{ref}	25 mm
δ^*_{ref}	7.0 mm
θ_{ref}	1.3 mm

TABLE 1. Incoming flow parameters taken at $x = -38.1$ mm

The effects of bulk compression are not so well known. In a compressible flow, bulk compression will occur whenever an adverse pressure gradient is present, but the effects are difficult to distinguish. Typically, an initial decrease in the skin friction occurs, followed by a recovery downstream (Peake, Brakmann & Romeskie 1971). In addition, Waltrup & Schetz (1973), Gootzait & Childs (1977) and Acharya, Kussoy & Horstman (1978) found that the turbulence activity increased throughout the boundary layer.

In supersonic flows, when the wall is curved (a configuration similar to that adopted for the current work), the effects of concave curvature act, in addition to the effects of bulk compression, and adverse pressure gradient. Previous investigations with these types of flows include the experiments of McLafferty & Barber (1962) and Hoydysh & Zakkay (1969). The most complete experiments, however, were performed by Sturek & Danberg (1972*a*, *b*) and Laderman (1980). Sturek & Danberg found that the velocity profiles continued to show a logarithmic region throughout the curvature. In contrast, Laderman observed deviations from the log-law which he attributed to an increase in the mixing length. Otherwise, both investigations found essentially similar results. The flows remained nominally two-dimensional and seemingly free of the longitudinal roll-cells observed in corresponding subsonic flows. The shear stress profiles, deduced from the mean flow results, displayed a maximum which moved away from the wall.

Nonetheless, the simultaneous action of concave curvature, adverse pressure gradient and compression are still not well understood. Direct measurements of the turbulence behaviour in this configuration have not been reported. Also, past experience has shown that the strong interactions that occur with these simultaneous extra strain rates can be extremely complex. For example, Smits, Young & Bradshaw (1979) found that a boundary layer experiencing the simultaneous effects of concave curvature and streamline divergence did not exhibit the turbulence amplification expected if each effect added linearly, nor did it show any evidence for the presence of longitudinal roll-cells (see also Smits & Joubert 1982; Smits & Wood 1985). Apparently, the amplification of longitudinal vorticity by concave curvature (through a Taylor–Görtler-like mechanism), and the amplification of spanwise vorticity by divergence (as described by Green) interact non-linearly to prevent the formation of steady longitudinal vortices.

The current two experiments as well as an earlier compression ramp study investigate, for a given perturbation strength, the effect of varying the perturbation rate. Specifically, all three experiments used the identical incoming boundary-layer

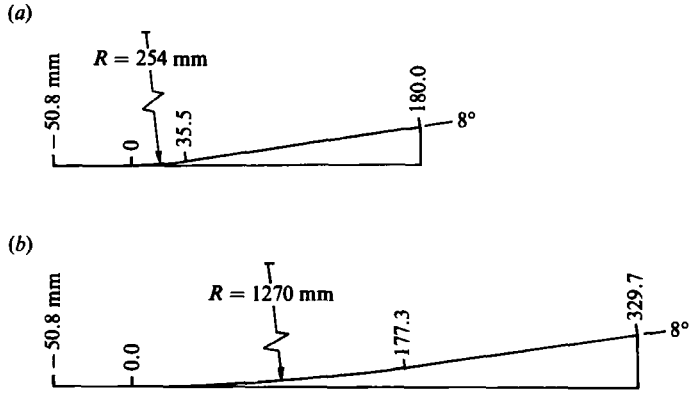

FIGURE 2. Model contours of 8° compression with concave surface curvature: (*a*) Model I, $\delta_{ref}/R = 0.10$; (*b*) Model II, $\delta_{ref}/R = 0.02$. All dimensions in mm.

and upstream-flow conditions (see table 1). In each case, the upstream boundary layer was allowed to develop fully under a nominally zero pressure gradient on the wind tunnel floor before entering a short region of surface curvature. Two different constant radii curved surfaces were used, corresponding to ratios of δ_{ref}/R of approximately 0.1 and 0.02 respectively, where δ_{ref} is the initial boundary-layer thickness. For both models, the total turning angle was fixed at 8°, and therefore the streamline deflection was the same as for the 8° ramp flow, and the overall pressure rise was almost identical (the pressure ratio for an 8° turning at Mach 2.87 by a shock is 1.758, compared with the isentropic value of 1.760). Thus, these three experiments test the response of the boundary layer to a wide range of stress gradients, that is, a wide range of strain rates while keeping the overall pressure rise and turning angle almost the same in each case.

The experimental methods and data reduction techniques are described in more detail in §2. The results, with some preliminary discussions are presented in §3, where a comparison with the 8° corner flow is also given. The comparison suggests that the compression corner and the short radius models present a 'rapid' perturbation to the boundary layer; rapid in the sense that the effect of the perturbation can be described in terms of total strains rather than local strain rates. In contrast, the flow on the large radius model is more complicated, and the local variations in the strain rates become important. The conclusions and final discussion are presented in §4, together with some suggestions regarding the calculation of these flows using a rapid distortion approach.

2. Experimental procedure

The experimental work was carried out in the Princeton University high Reynolds number 20 × 20 cm supersonic blowdown wind tunnel. The models were installed on the tunnel floor 1149 mm from the nozzle exit.

The stagnation pressure was 6.9×10^5 N/m^2 (100 p.s.i.a.), and the incoming flow had a free-stream Mach number of 2.87 ± 0.02 with a unit Reynolds number of approximately 6.3×10^7/m. The wall conditions were near adiabatic. The incoming turbulent boundary layer developed in a zero pressure gradient, and just upstream of each model the boundary-layer thickness δ_{ref} was about 25 mm and the Reynolds number based on momentum thickness was approximately 77 600 (see table 1). The

r.m.s. free-stream turbulence level, expressed as a fraction of the free-stream mass-flow, was about 1%.

The models are shown in figure 2. Both models had a curved region with an overall turning angle of 8° followed by a 152 mm flat plate recovery section. The curved portions had radii of curvature $R = 254$ mm and $R = 1270$ mm giving $\delta_{\text{ref}}/R = 0.10$ (Model I) and $\delta_{\text{ref}}/R = 0.02$ (Model II), respectively. The width of each model was 152 mm, allowing a 25 mm gap on each side for the passage of the tunnel sidewall boundary layers, and aerodynamic fences were fitted to improve the two-dimensionality of the flow. The fences were formed by thin parallel plates shaped so that they extended at least 25 mm above the surface of the model. The leading edges were swept back at 45°, and all edges were sharp.

To measure the mean flow profiles, Pitot pressure, static pressure and total temperature probes were used. The profiles were measured normal to the local model surface, at a position 13 mm off the tunnel centreline. The x-coordinate was defined as the streamwise direction and it was measured along the surface of the model with the origin at the beginning of curvature. The y-coordinate was measured normal to the wall.

The local skin friction was found using a Preston tube. A circular tube was used with an outside diameter of 1.6 mm, and an inner-to-outer diameter ratio of 0.6, and the measurements were reduced according to the method suggested by Hopkins & Keener (1966). Due to the complexity of the flow, and the uncertainty in defining boundary-layer edge conditions, 'effective' edge conditions, obtained from tunnel stagnation and local wall static pressures were used to define the skin friction coefficient (as first suggested by Settles *et al.* 1979).

In addition to Preston tube measurements, values of C_f were obtained from the velocity profiles by using the Van Driest transformation and fitting the transformed velocity profiles to the standard logarithmic law, assuming that the log-law applies in a region close to the surface. Since the relaxation times close to the wall are very short, we expect the flow close to the surface to quickly adjust to the new boundary conditions and follow a logarithmic distribution.

Further details of the models, the experimental procedures and mean flow data analysis are given by Taylor (1984).

For the turbulence measurements, DISA 55M10 constant-temperature anemometers were used according to the techniques outlined by Smits, Muck & Hayakawa (1983) and Smits & Muck (1984). A normal wire was used to measure the longitudinal component of the mass-flow fluctuations $\overline{(\rho u)'^2}$, and a single inclined wire was used to measure the mass-weighted shear stress component $\overline{(\rho u)'v'}$. In all respects, the hot-wire and data-acquisition techniques were the same as those described in the compression corner study by Smits & Muck (1987) but for the sake of completeness the most pertinent information is repeated here.

Briefly, each anemometer was operated at an overheat ratio of about 1.0, and the contribution of the total temperature fluctuation to the signal was neglected. Hence, the output was assumed to be sensitive to mass-flow fluctuations only, an assumption that leads to an overestimate of the mass-flow intensity by about 4% in the middle of the upstream boundary layer (Smits *et al.* 1983). The wires were calibrated for mass-flow sensitivity in a small Mach 3 pilot tunnel by changing the stagnation pressure. The inclined wire was calibrated for directional sensitivity by yawing the probe through an angle of $\pm 10°$ from its null position. The wires were not calibrated in the subsonic and transonic regimes. According to Rong, Tan & Smits (1985), the mass-flow sensitivity of the normal wire is independent of Mach number. However,

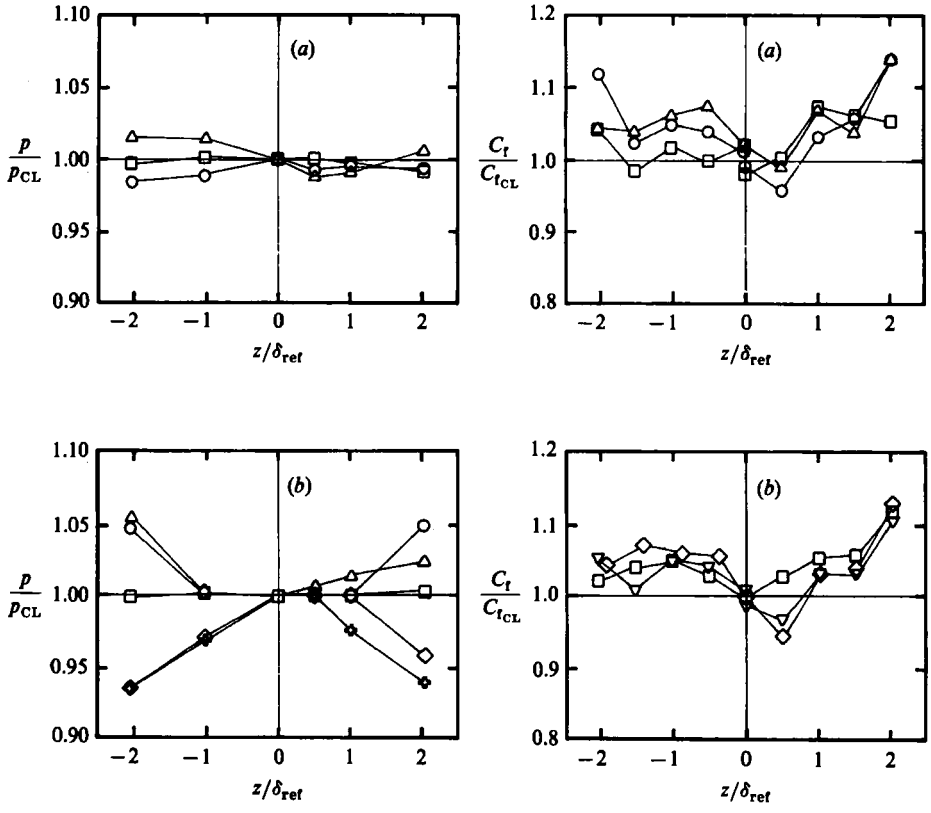

FIGURE 3. Spanwise static pressure and skin friction distributions for (*a*) Model I, (*b*) Model II. All values non-dimensionalized by centreline value: □, $x = -25$ mm; △, 63 mm; ▽, 152 mm; ○, 178 mm; ◆, 215 mm; ◇, 293 mm.

the directional sensitivity of an inclined wire is a strong function of Mach number in the transonic regime, and its calibration is valid only where the local Mach number in the direction normal to the wire filament exceeds 1.2. Hence, the inclined wire measurements near the wall must be treated with caution.

Following appropriate filtering, the mean and fluctuating components of the hot-wire signal were digitized directly at sampling rates of 50 kHz and 500 kHz respectively, and all further processing was carried out using a Hewlett–Packard HP1000 minicomputer. The instantaneous value of the anemometer voltage was directly converted to the instantaneous value of mass flow by inverting the calibration curve, thereby avoiding the use of sensitivity coefficients. The instantaneous mass-flow fluctuations were found by subtracting the time-averaged mass flow from the total instantaneous mass flow. The system frequency response was limited by the spatial and temporal resolution of the hot wire. According to Wyngaard (1968), for a typical wire length of 0.8 mm, the measured one-dimensional spectrum at $y/\delta = 0.5$ falls to one-half its true value at about 250 kHz. A more severe restriction is the maximum frequency response of the anemometer, and a typical upper limit was 125 kHz.

The velocity fluctuations were obtained from the mass-flow fluctuations by assuming Morkovin's (1962) 'Strong Reynolds Analogy' which requires that the pressure fluctuations and total temperature fluctuations are small. Under these

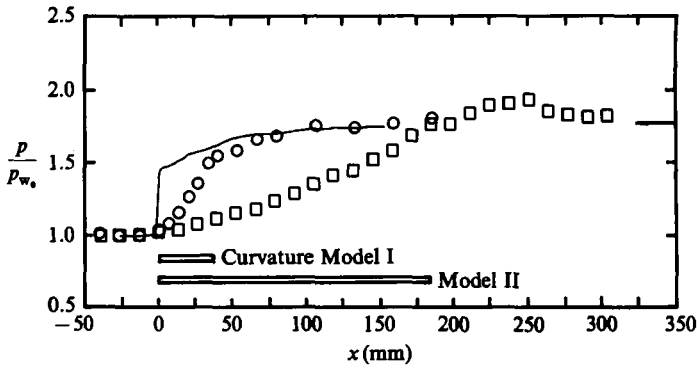

FIGURE 4. Streamwise static pressure distributions for ○, Model I; □, Model II; ——, 8° ramp. The inviscid pressure rise for an 8° compression is indicated on the right-hand side.

conditions, the r.m.s. velocity fluctuation level is proportional to the r.m.s. mass-flow fluctuation level. The validity of this assumption was discussed by Dussauge & Gaviglio (1981) and Smits *et al.* (1983), and for the present experiments the accuracy seems acceptable.

3. Results and discussion

To investigate the two-dimensionality of the flow, the spanwise variations of wall static pressure and skin friction were measured at three streamwise stations (see figure 3). The spanwise variations for both models were small, and did not seem to be amplified by the curvature. In addition, surface flow patterns on both models showed that surface streamlines remained nearly parallel, and therefore no evidence for the presence of steady longitudinal vortices was found. It is possible that unsteady vortices formed, without a preferred spanwise position, but this possibility was not investigated.

The surface static pressure distributions for the 8° ramp, Model I, and Model II are shown in figure 4. The 8° ramp shows an abrupt jump in pressure at $x = 0$ followed by a slower increase up the inviscid level, corresponding to a decrease in Mach number from 2.87 to 2.48. Model I shows a much more gradual pressure rise, occurring over a distance of approximately twice the length of the curved region before levelling off to about the inviscid value. For Model II, the pressure reaches the inviscid level at the end of the curved region, overshoots by approximately 15% and then returns to the inviscid level by the end of the recovery region. It is not clear if the overshoot is a result of the curvature. The experiments and calculations by Roshko & Thomke (1969) showed that similar pressure overshoots occurred for high Reynolds number two-dimensional ramp flows over a range of Mach numbers. In the present case, however, the pressure distribution for the 8° ramp and Model I displayed no overshoot, whereas the Model II distribution did. It is possible that this behaviour for Model II was caused by a spurious wave system generated by the tunnel walls. However, a careful study failed to reveal a likely source for this wave system, and the overshoot was accepted as part of the flow response.

The skin friction coefficients for all three models are given in figure 5. The ramp results show an initial drop of approximately 40%, followed by a gradual increase which continues to the downstream end of the model. Similarly, both curved models display a decrease in C_f in the curved region followed by a gradual increase in the

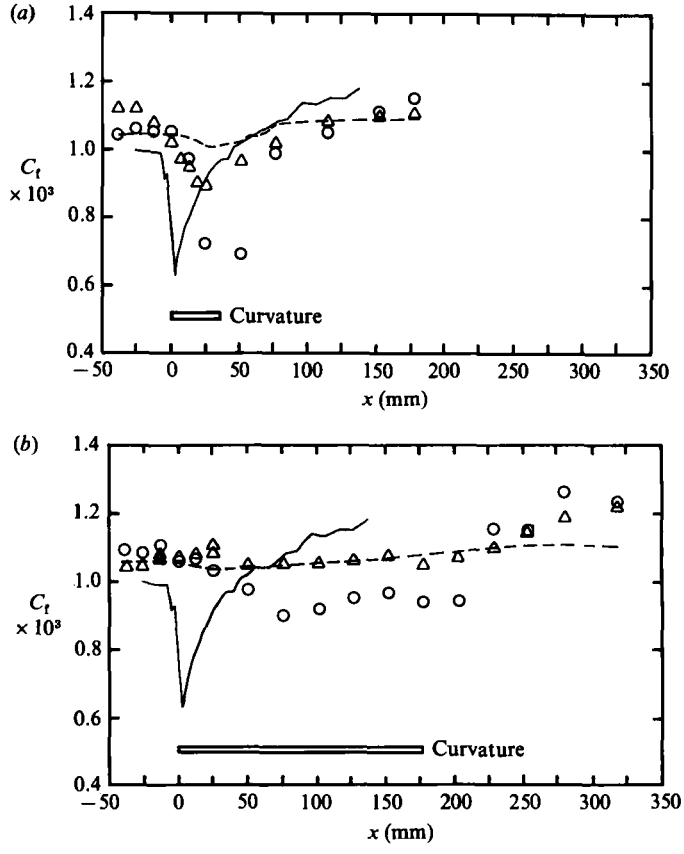

FIGURE 5. Streamwise skin-friction distributions for (*a*) Model I, (*b*) Model II. ○, Clauser chart from transformed velocity profiles; △, Preston tube (Hopkins & Keener 1966); ——, skin friction according to Van Driest (1951); ——, 8° ramp experimental results.

recovery region. In both cases, the skin friction eventually rises above the self-preserving level but the models are too short to allow full relaxation. The results derived from transformed velocity profiles and Preston tube measurements agree well upstream and downstream of the curvature. In the curved region, however, differences up to 25 % are observed. The discrepancies illustrate how difficult it is to measure accurate skin friction values in adverse pressure gradient, compressible boundary layers. For example, the comprehensive survey by Fernholz & Finley (1980) showed that differences up to $\pm 15\,\%$ between the skin friction derived from Preston tubes and velocity profiles were commonly encountered.

The downstream development of boundary-layer thickness, displacement thickness, and momentum thickness are shown in figures 6 and 7. The behaviour of each parameter is qualitatively the same for all three flows. The boundary-layer thickness decreases in response to the adverse pressure gradient, and it then increases gradually in the recovery region. A similar trend is seen in the displacement thickness distributions. The momentum thickness variation is more or less as expected: it increases where the pressure is varying and then levels off in the region of zero pressure gradient.

The transformed velocity profiles in log–law coordinates are given in figure 8. The friction velocity was chosen such that the profiles for all three cases followed the log-law close to the wall. Further from the wall, however, the downstream profiles

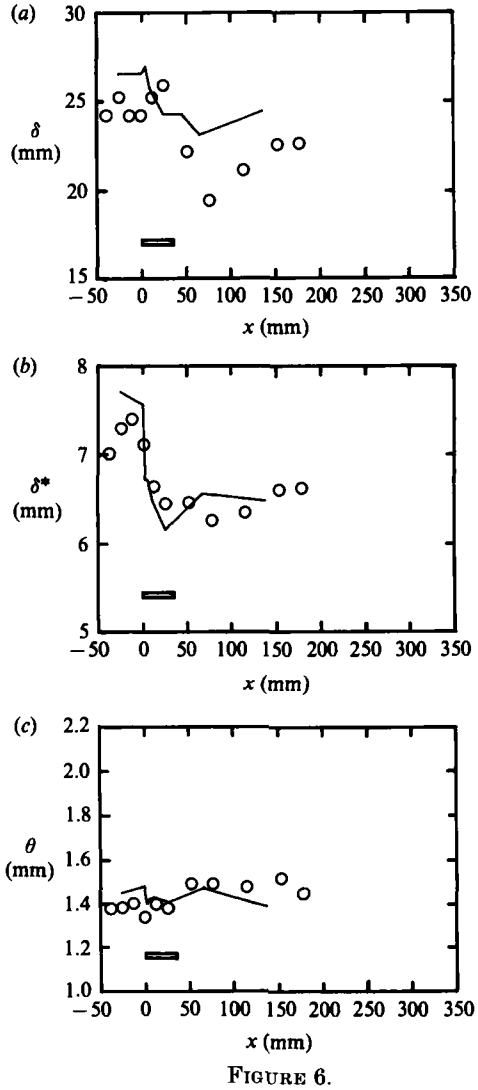

FIGURE 6.

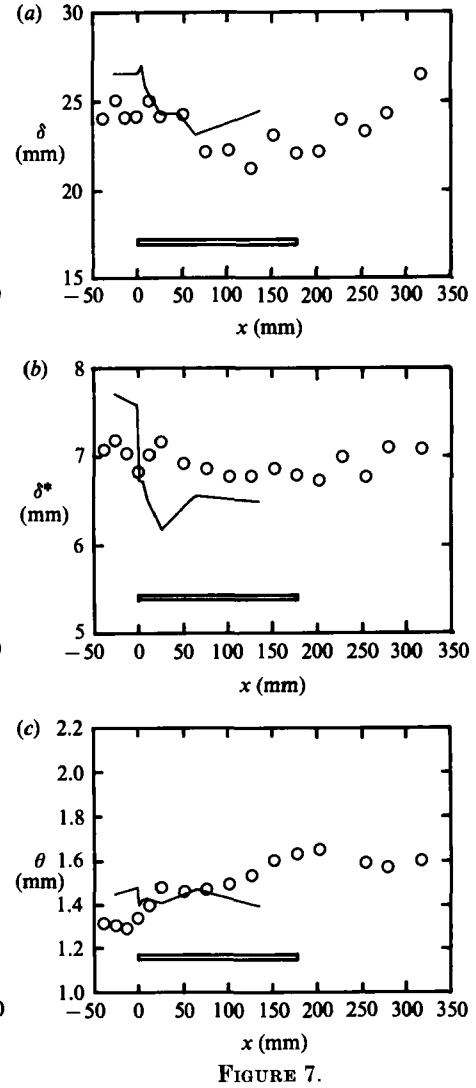

FIGURE 7.

FIGURE 6. Distribution of (*a*) boundary-layer thickness, (*b*) displacement thickness, (*c*) momentum thickness for ○, Model I; ——, 8° ramp. Horizontal bar indicates extent of curved wall.

FIGURE 7. Distribution of (*a*) boundary-layer thickness, (*b*) displacement thickness, (*c*) momentum thickness for ○, Model II; ——, 8° ramp. Horizontal bar indicates extent of curved wall.

fall below the logarithmic velocity distribution. This characteristic 'dip' was also found in subsonic flows with short regions of concave surface curvature (Smits, Young & Bradshaw 1979), and in subsonic flows with lateral divergence and concave curvature (Smits, Eaton & Bradshaw 1979). Smits *et al.* suggested that this dip indicates that the dissipation length scale increases faster with distance from the wall than in the corresponding equilibrium flow.

The turbulence measurements include the longitudinal mass-flow fluctuations $\overline{(\rho u)'^2}$, the mass weighted shear stress $\overline{(\rho u)'v'}$, and the turbulent stresses $\bar{\rho}\overline{u'^2}$ and $\bar{\rho}\overline{u'v'}$. The upstream reference conditions are used as non-dimensionalizing variables throughout, and hence the results reflect the behaviour of the absolute levels.

The general behaviour of the longitudinal component of the turbulence intensity

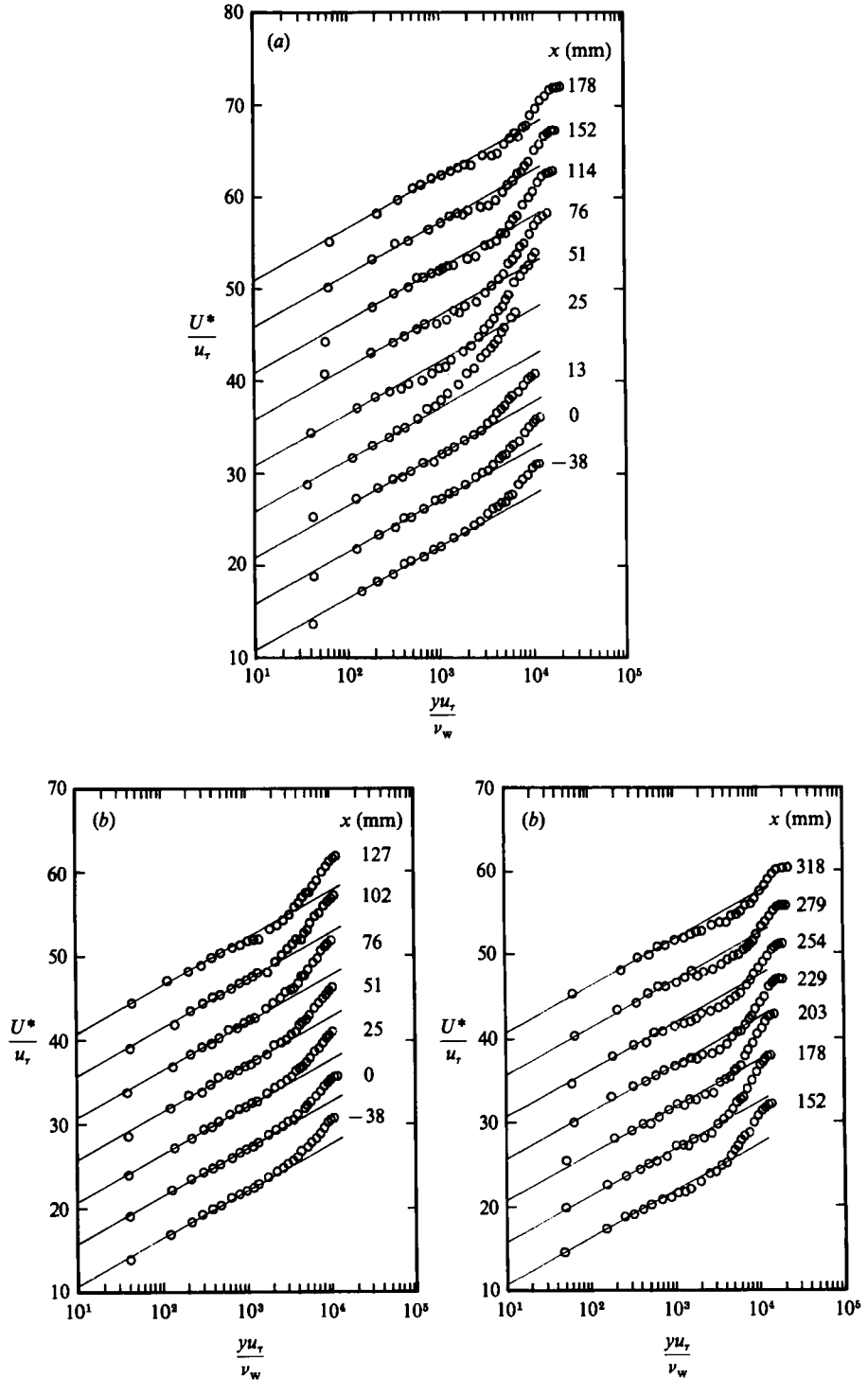

FIGURE 8(*a*, *b*). For caption see facing page.

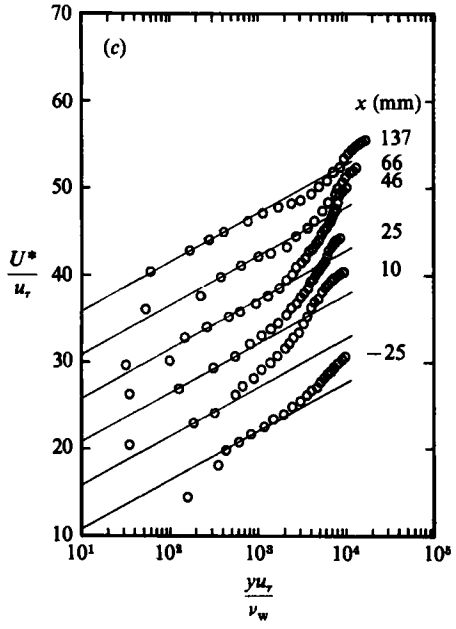

FIGURE 8. Velocity profiles using Van Driest (1951) transformation (*a*) Model I, (*b*) Model II, (*c*) 8 degree ramp.

is very similar in all three cases (see figure 9). Initially, there is a rapid amplification of $\bar{\rho}\overline{u'^2}$ through the perturbation zone. This increase continues further downstream, and the peak amplification is about fourfold in each case. In the outer part of the boundary layer, there is little sign of recovery or relaxation but near the wall the intensities quickly fall, indicating that the relaxation process begins at the wall and propagates outward.

The variation of the shear stress $\tau = -\bar{\rho}\overline{u'v'}$ is shown in figure 10. Again, a considerable amplification occurs through the perturbation zone, continuing into the downstream region, and the relaxation appears to propagate outwards from the wall. However, the peak amplification levels for the three cases differ considerably; for the compression corner and Model I it is about fourfold, whereas for Model II it is only about twofold.

To verify the hot-wire results, the shear stresses were also found from the mean flow measurements by integrating the equations of motion (see Taylor 1984 for details). Upstream of the curvature, the comparison with the hot-wire data and Sandborn's (1974) 'best estimate' was very satisfactory (figure 11). Downstream, the streamwise gradients are severe, and the accuracy of the calculations was only acceptable for Model II. The peak stress levels are in reasonable agreement throughout the flow and the comparison with the hot-wire results is qualitatively encouraging. The hot wire, however, always shows the peak in the shear stress at a greater distance from the wall. It appears that the true stress levels probably lie between the two results, since the errors associated with the mean flow analysis are considerable and the inclined hot-wire results are inaccurate near the wall.

Even if the shear stress levels are in some doubt, the amplification of $\bar{\rho}\overline{u'v'}$ and $\bar{\rho}\overline{u'^2}$ are clearly different. This observation is rather surprising in that stress ratios, such as $a_1'' = -\overline{u'v'}/\overline{u'^2}$, and $a_1 = -\overline{u'v'}/\overline{q'^2}$, where $\overline{q'^2}$ is (twice) the turbulent kinetic energy, often display significantly less variation than the stresses themselves, and

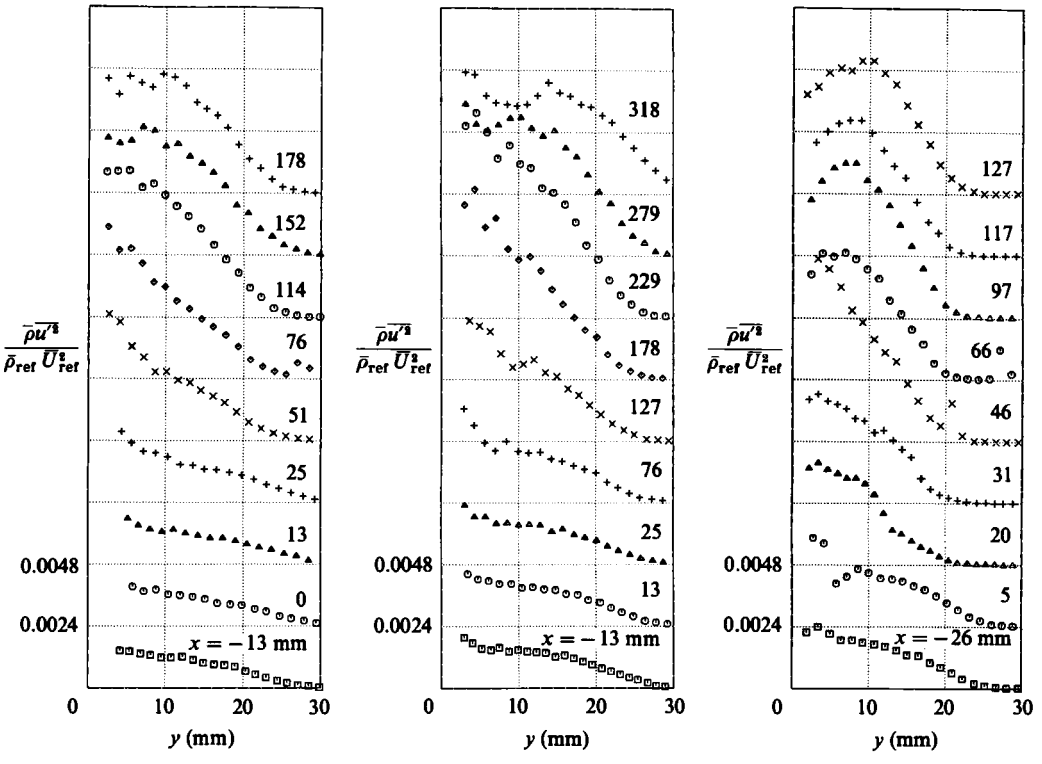

FIGURE 9. Longitudinal turbulent stress profiles for (*a*) Model I, (*b*) Model II, (*c*) 8° ramp.

these 'structure parameters' are therefore normally useful in modelling the turbulence behaviour. However, the experimental results for a_1'', shown in figure 12, do not support these expectations, at least for the compression corner and Model I. Furthermore, the measurements by Ardonceau *et al.* (1979) showed that the anisotropy ratio $\langle v' \rangle / \langle u' \rangle$ decreased considerably through a shock/boundary interaction because of the time taken to redistribute the increased energy among the three components. Hence it appears that the levels of a_1 may vary even more than a_1''.

The present results show that, despite the scatter, the behaviour of these structure parameters is clearly a function of the perturbation rate. For the compression corner and Model I, where the perturbation is comparatively rapid, a_1'' increases by about 50 % in the middle of the boundary layer. When the perturbation is more spread out, as in Model II, we see that this ratio remains nearly constant throughout the curvature.

The mixing length profiles were calculated using the hot-wire results and the smoothed velocity profiles. The results are shown in figure 13 and the results display considerable scatter, as might be expected. Nevertheless, the upstream profile agrees well with Klebanoff's (1955) curve. Downstream, the mixing length increases considerably. Near the wall, in particular, there is a noticeable increase in the slope supporting the earlier observation that the lengthscales near the wall increase faster with distance from the wall than in the self-preserving case.

The energy spectra for the mass-flow fluctuations are shown in figure 14, in the form of frequency times energy density versus the logarithm of the frequency. The area under each curve is therefore directly proportional to the energy content of

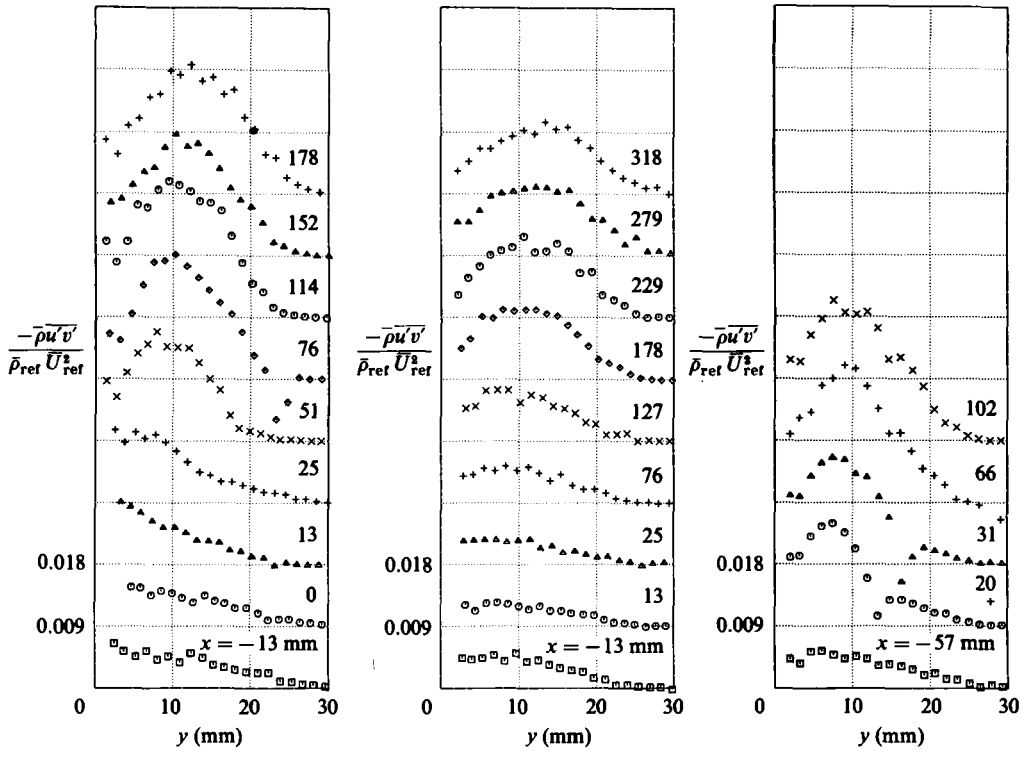

FIGURE 10. Shear stress profiles for (*a*) Model I, (*b*) Model II, (*c*) 8° ramp.

the longitudinal turbulence component, and the peak corresponds to the frequency of the most energetic motions, f_e. The spectra are shown for streamlines originating at three y/δ positions for one upstream and one downstream location along Models I and II. The spectra clearly show the amplification of the turbulence levels, as well as dislaying a shift in energy content, especially near the wall. The shift in f_e is plotted as a function of streamwise distance in figure 15.

Perry, Lim & Henbest (1985) argued that near the wall in an undisturbed boundary layer, at moderate to high wave numbers (which includes the point where the energy spectrum has a maximum), a region exists in wavenumber space where universal wall motions dominate. These motions depend on distance from the wall, and therefore f_e should scale with U/y. However, in the current work, near the wall, it appears that the wall motions have a much larger scale than that observed in a self-preserving boundary layer. The innermost streamline is located in the region of the velocity profile where the dip below the logarithmic line was observed, and the earlier observation that the lengthscale of the turbulent motions in this region was increased by the overall perturbation is therefore substantiated by the spectral measurements. In contrast, in the outer part of the boundary layer, the spectra show little change in frequency content.

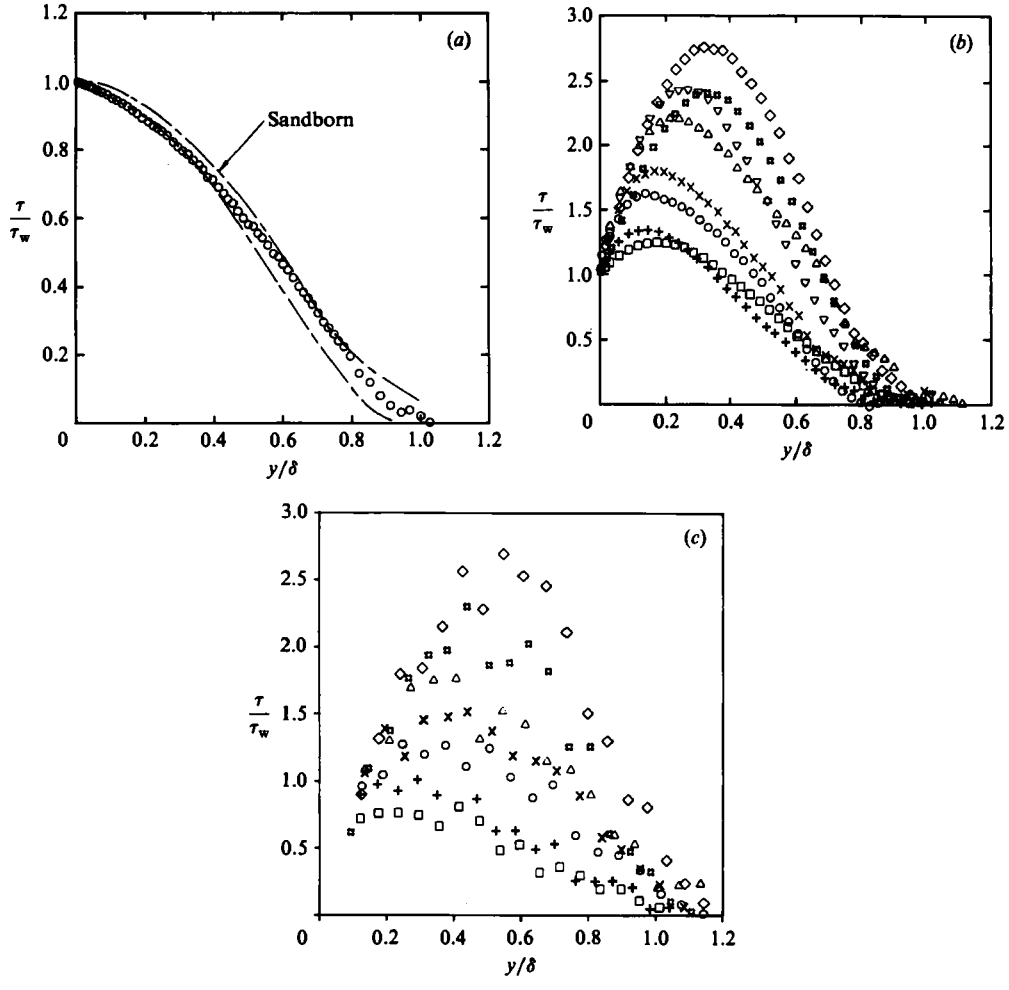

FIGURE 11. Turbulent shear stress derived from mean velocity profiles for (*a*) upstream boundary layer, (*b*) Model II. For comparison, the hot-wire results are plotted in (*c*). □, $x = 25$ mm; +, 51; ○, 76; ×, 102; △, 127; ▽, 178; ◇, 203; ⊠, 229.

4. Implications for computations

Numerical calculations of strongly perturbed flows such as the present one are few in number. Recent calculations by Degani & Smits (1985) for Models I and II with a one-equation turbulence model showed encouraging agreement with the measured skin friction distributions. Other calculations for similar flows have used turbulence models ranging from a mixing-length approach to a full Reynolds-stress model. However, none of these calculations were able to predict both the mean velocity profiles and the skin friction distribution accurately. Predictions of turbulence quantities have met with an even lesser degree of success. On the whole, these computations demonstrate that the prediction of complex, compressible flow may require new approaches.

Specifically, these experiments suggest that the flow field distortion may be described using rapid distortion concepts since the results indicate that the Model I flow and the ramp flow respond in a very similar way. This behaviour suggests that

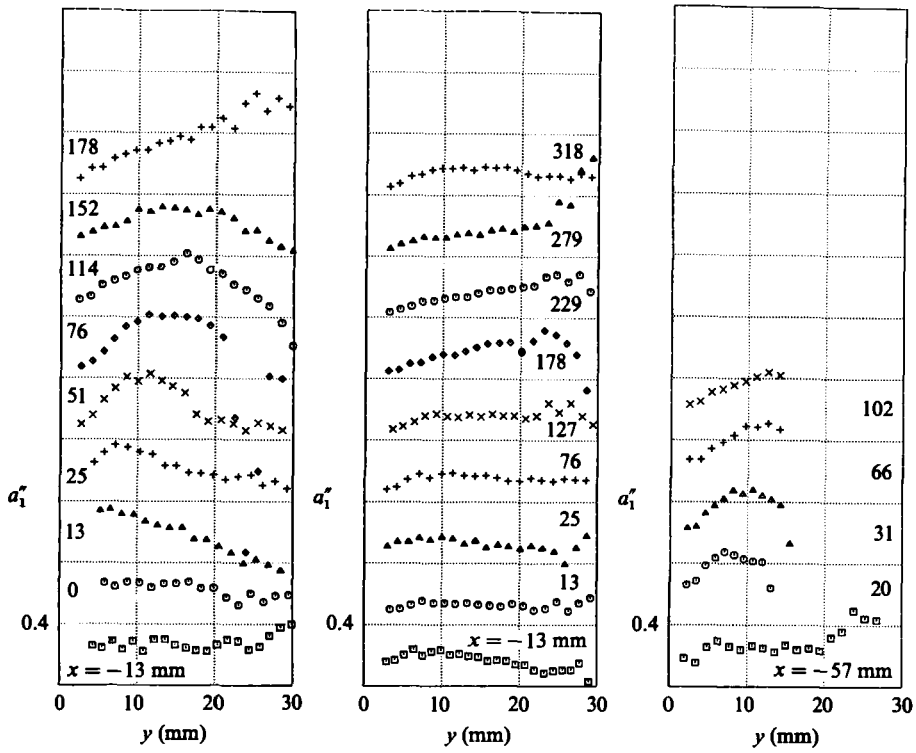

FIGURE 12. Profiles of non-dimensional structure parameter a_1'' for (*a*) Model I, (*b*) Model II, (*c*) 8° ramp.

the response depends on the total strain applied, rather than the nature of the strain-rate distribution.

A distortion is 'rapid' if it is applied to a turbulent field during a time which is much smaller than the characteristic turbulence timescale (Hunt 1977). That is

$$\frac{L/\Lambda}{q'/U} \ll 1,$$

where Λ is the characteristic turbulent lengthscale, and L/U is the time of the flight of a fluid particle in a distortion of length L. If this condition is satisfied, the rate of dissipation of turbulent kinetic energy per unit mass can be treated as a constant, equal to its value upstream of the distortion, and the turbulence distortion is mainly due to changes in the mean flow. To a first approximation, the dissipation, diffusion and the return to isotropy terms may be neglected. However, the 'rapid part of the pressure' needs to be modelled, and four different models have been proposed: Naot, Shavit & Wolfshtein (1970), Launder, Reece & Rodi (1975), Lumley (1975) and Shih & Lumley (1987).

Jayaram, Dussauge & Smits (1985) recently tested these concepts in a calculation of the Model I flow. The method of characteristics was used to calculate the mean flow, and the results were in good agreement with the experiment, particularly in the middle of the layer. Hence, in this region, the turbulence should not affect the mean flow behaviour significantly, as expected from the observation that $\partial\tau/\partial y \ll \partial p/\partial x$. Similar results were obtained by Roshko & Thomke (1969) and Rosen, Roshko &

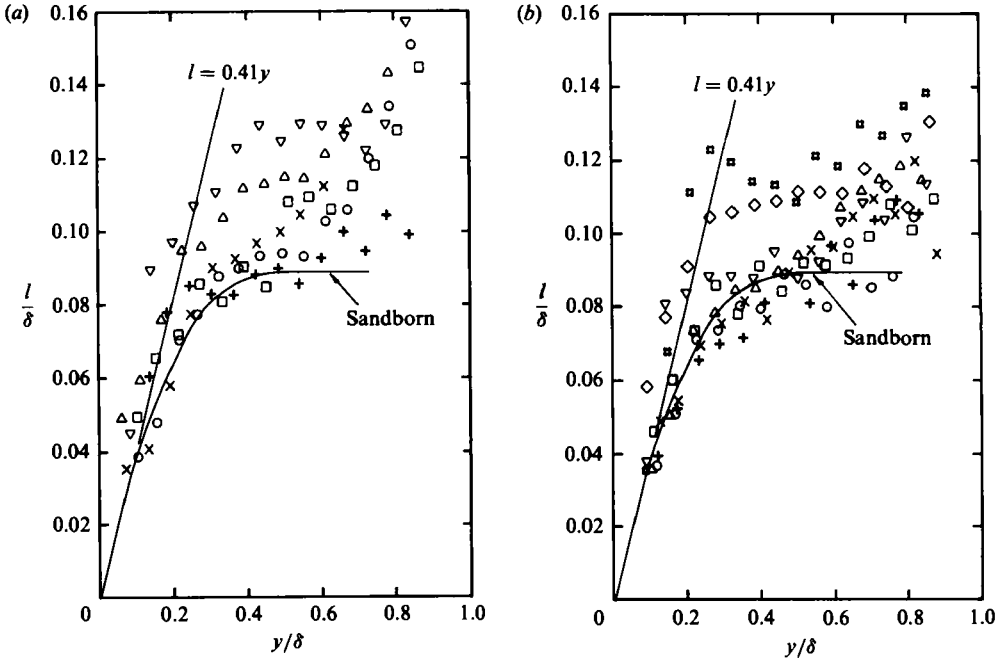

FIGURE 13. Mixing length derived from hot-wire and mean velocity profiles for (*a*) Model I: □, $x = -13$ mm; +, 13; ○, 25; ×, 76; △, 114; ▽, 152; (*b*) Model II: □, $x = -13$ mm; +, 25; ○, 76; ×, 127; △, 178; ▽, 229; ◇, 279; ■, 318.

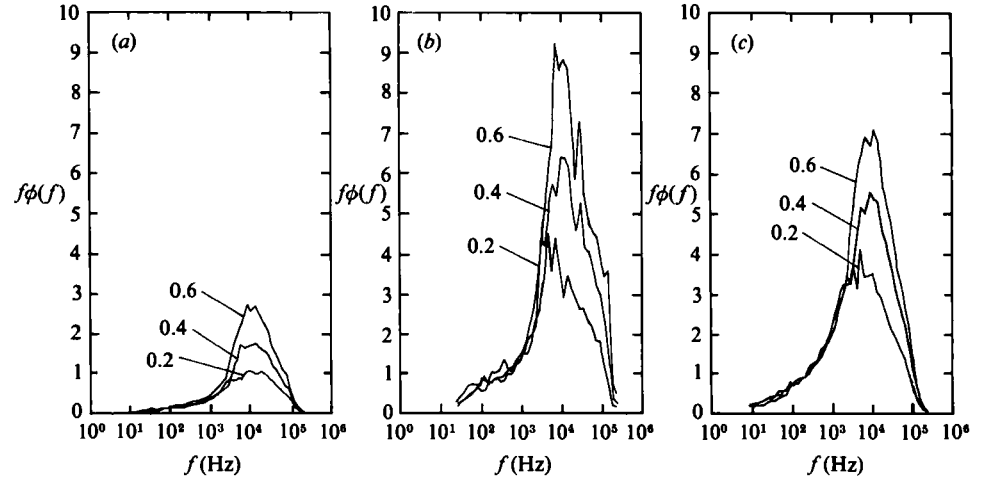

FIGURE 14. Energy spectra along streamlines originating at $y/\delta_{\text{ref}} = 0.2$, 0.4 and 0.6. (*a*) upstream of curvature ($x = -13$ mm). (*b*) Model I, 77 mm downstream of end of curvature ($x = 113$ mm). (*c*) Model II, 77 mm downstream of end of curvature ($x = 254$ mm).

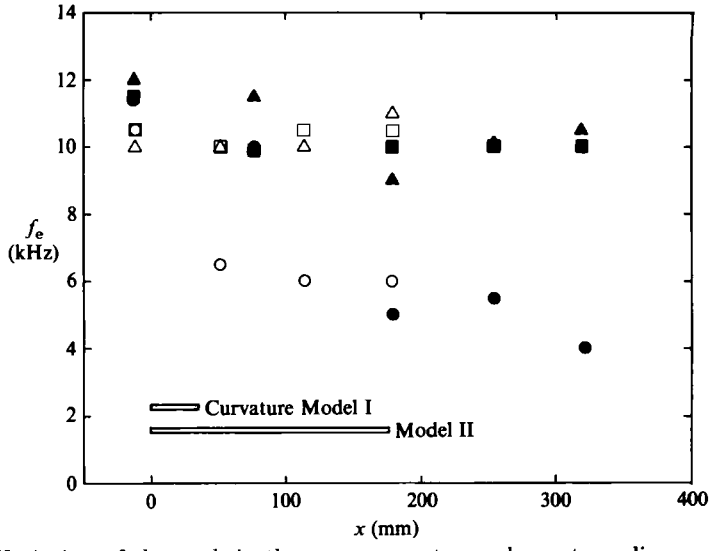

FIGURE 15. Variation of the peak in the energy spectrum along streamlines originating at: ○, $y/\delta_{\text{ref}} = 0.2$; □, $y/\delta_{\text{ref}} = 0.4$; △, $y/\delta_{\text{ref}} = 0.6$. Open symbols: Model I; closed symbols: Model II.

Parish (1980) for attached compression ramp flows, and by Dussauge & Gaviglio (1981) for a rapidly expanded flow.

Calculations of kinematic stresses were then performed along three different streamlines using all four of the above models for the rapid part of the pressure. Although the best overall performance was demonstrated by the Shih & Lumley model, all calculations predicted the turbulent stresses well along a streamline which originated in the middle of the boundary layer. Closer to the wall, all models gave good results in the region of curvature but further downstream the results were sensitive to the modelling of the rapid part of the pressure term. Still closer to the wall, the calculated results diverged from the measured values, partly because of experimental inaccuracies, and partly because of the breakdown of the rapid distortion assumptions. Thus neglecting the dissipation, diffusion and the return to isotropy seems acceptable for regions not too close to the wall.

By way of contrast, in the case of a rapid expansion (Dussauge & Gaviglio 1981) calculations using three different models for the rapid part of pressure all gave essentially the same predictions for the decrease in $\overline{u'^2}$. In the present case, the differences observed may be due to the larger influence of the mean shear and the pressure gradient experienced by the flow. More importantly, it suggests that the rapid part of the pressure must be modelled with care; neglecting these terms in calculating rapidly perturbed flows is certainly not justified.

5. Discussion and conclusions

An experimental investigation of a compressible turbulent boundary layer subjected to a short region of longitudinal surface curvature and adverse pressure gradient was presented. The velocity profiles displayed a 'dip' below the log–law, suggesting an increase in the turbulence lengthscale, and no evidence was found for the presence of longitudinal roll-cells as might be expected to occur in concavely curved shear layers. In both these respects, the flow was similar to the incompressible

flow studies by Smits *et al.* (1979), who investigated the response of a boundary layer to the combined effects of concave curvature and lateral divergence. In the present flow, the boundary layer experiences the combined effects of concave curvature and bulk compression, and it appears that the combined effects of curvature and either divergence or compression lead to a rather similar response.

As far as the turbulence behaviour is concerned, the compression corner and Model I influenced the turbulence in an almost identical manner. This result suggests that the perturbation in these two cases is sufficiently rapid to alter the turbulence in a manner which depends only on the overall changes that occur, not on the path taken. The parameter describing this 'change of state' is therefore the total strain, that is, the integral of the strain rate over the time it acts. For curvature, this integral is equal to the total turning angle, and for compression it is approximately equal to $(1/\gamma)\ln(p_2/p_1)$, where p_2/p_1 is the pressure ratio. It appears that the shock wave itself has no explicit effect on the turbulence but this conclusion can only hold if the shock is relatively weak, such that compression is approximately isentropic, and separation, with its associated unsteadiness is absent. These conditions seem to be satisfied in the 8° compression corner experiment.

The response to the perturbation produced by Model II is quite different to that seen in the other two experiments. For example, the stress ratio $-\overline{u'v'}/\overline{u'^2}$ is relatively unaffected. Hence, despite the large amplification of the absolute turbulent stresses, the turbulence structure is not significantly altered. In this case, the local strain rates are probably more useful than the total strain for describing the response of the turbulence.

Close to the wall, we observed the beginning of a relaxation process in all three experiments. It is to be expected that the flow near the wall will attain equilibrium more quickly than the flow in the outer part of the layer; a measure of the large eddy time constant is the turbulent energy divided by its rate of production, and this will vary approximately as $1/(\partial U/\partial y)$ (Townsend 1976). This relaxing region grew in size as we proceeded downstream, and its growth resembled that of a new boundary layer. Similar 'internal layers' have been observed in boundary layers perturbed by sudden changes in surface roughness, surface curvature, and pressure gradient (Smits & Wood 1985) and the similarity displayed by the propagation of the relaxation outward from the wall may be useful in a qualitative understanding of the flow behaviour in the present experiments.

For this Mach number, and this turning angle, a compression corner and a short radius concavely curved wall (Model I) affect the turbulence in an almost identical fashion. Hence, we class these perturbations as rapid, in the sense that they are characterized by the total strain imposed on the turbulence, and that they are independent of the nature of the perturbation itself.

Unfortunately, these compressible flow experiments are all confined to the region in the vicinity of the distortion, and the measurements downstream of the distortion only capture the start of the relaxation. At present, no information is available on the nature of the recovery process, and therefore no conclusions can be made regarding the far-downstream behaviour. Experiments which are specifically designed to investigate this aspect are urgently required. A new facility, currently under construction at Princeton with the support of the DOD University Research Instrumentation Program, will allow some of these experiments to be performed.

The experimental work was supported by NASA Headquarters Grant NAGW-240, monitored by Dr Gary Hicks. The analysis of the data and the preparation of this

paper was supported by NASA Langley Grant NAGl-545, monitored by Dr Wallace Sawyer.

REFERENCES

ACHARYA, M., KUSSOY, M. I. & HORSTMAN, C. C. 1978 Reynolds number and pressure gradient effects on compressible turbulent boundary layer. *AIAA J.* **16**, 1217–1218.

ARDONCEAU, P. L., LEE, D. H., ALZIARY DE ROQUEFORT, T. & GOETHALS, R. 1979 Turbulence behaviour in shock wave/boundary layer interaction. *AGARD Conf. Proc.* 271, paper 8.

BRADSHAW, P. 1973 Streamline curvature effects in turbulent flow. *AGARDograph* 169.

BRADSHAW, P. 1974 The effect of mean compression or dilatation on the turbulence structure of supersonic boundary layers. *J. Fluid Mech.* **63**, 449–464.

BRADSHAW, P., FERRISS, D. H. & ATWELL, N. P. 1967 Calculation of boundary layer development using the turbulent energy equation. *J. Fluid Mech.* **28**, 593–616.

DEGANI, D. & SMITS, A. J. 1985 Numerical study of the response of a compressible turbulent boundary layer to a short region of surface curvature. *AIAA paper* 85–1667.

DUSSAUGE, J.-P. & GAVIGLIO, J. 1981 Bulk dilatation effects on Reynolds stress in the rapid expansion of a turbulent boundary layer at supersonic speed. *Proc. Symp. Turbulent Shear Flows, Davis, Calif.* vol. 2, pp. 33–38.

FERNHOLZ, H. H. & FINLEY, P. J. 1980 A critical commentary on mean flow data for two-dimensional compressible turbulent boundary layers. *AGARDograph* 253.

GOOTZAIT, E. & CHILDS, M. E. 1977 Turbulence measurements in axisymmetric supersonic boundary layer flow in adverse pressure gradients. *AIAA paper* 77–129.

HOPKINS, E. J. & KEENER, E. R. 1966 Study of surface Pitots for measuring turbulent skin friction at supersonic Mach numbers – adiabatic wall. *NASA Tech. Note* D-3478.

HOYDYSH, W. G. & ZAKKAY, V. 1969 An experimental investigation of hypersonic turbulent boundary layers in adverse pressure gradient. *AIAA J.* **7**, 105–116.

HUNT, J. C. R. 1977 A review of the theory of rapidly distorted turbulent flows and its applications. *Proc. Bienn. Fluid Dyn. Symp., 13th, Warsaw, Poland*, pp. 121–152.

JAYARAM, M., DUSSAUGE, J. P. & SMITS, A. J. 1985 Analysis of a rapidly distorted, supersonic, turbulent boundary layer. *Proc. 5th Symp. on Turbulent Shear Flows, Cornell University, Ithaca, NY.*

KLEBANOFF, P. S. 1955 Characteristics of turbulence in a boundary layer with zero pressure gradient. *NACA Rep.* 1247.

LADERMAN, A. J. 1980 Adverse pressure gradient effects on supersonic boundary-layer turbulent. *AIAA J.* **18**, 1186–1195.

LAUNDER, B. E., REECE, G. J. & RODI, W. 1975 Progress in the development of a Reynolds-stress turbulence closure. *J. Fluid Mech.* **68**, 537–566.

LUMLEY, J. L. 1975 Lecture, Von Karman Inst., Rhodes-St Genese.

MCLAFFERTY, G. H. & BARBER, R. E. 1962 The effect of adverse pressure gradient on the characteristics of turbulent boundary layers in supersonic streams. *J. Aero. Sci.* **29**, 1–10.

MORKOVIN, M. V. 1962 Effects of compressibility on turbulent flows. In *Mécanique de la Turbulence* (ed. A. Favre, pp. 367–380. Paris: CNRS.

MUCK, K.-C. 1982 *Turbulent boundary layers on mildly curved surfaces.* PhD. thesis, University of London, UK.

NAOT, D., SHAVIT, A. & WOLFSHTEIN, M. 1970 Interactions between components of the turbulent velocity correlation tensor. *Israel J. Tech.* **8**, 259.

PEAKE, D. J., BRAKMANN, G. & ROMESKIE, J. M. 1971 Comparisons between some high Reynolds number turbulent boundary layer experiments at Mach 4 and various recent calculation procedures. *AGARD Conf. Proc.* 93–71, paper 11.

PERRY, A. E., LIM, K. L. & HENBEST, S. M. 1985 A spectral analysis of smooth flat-plate boundary layers. *Proc. 5th Symp. on Turbulent Shear Flows Cornell University, Ithaca, NY*, pp. 9.29–9.34.

RAMAPRIAN, B. R. & SHIVAPRASAD, B. G. 1978 The structure of turbulent boundary layers along mildly curved surfaces. *J. Fluid Mech.* **85**, 273–303.

RONG, B. S., TAN, D. K. M. & SMITS, A. J. 1985 Calibration of the constant-temperature normal hot-wire anemometer in transonic flow. *Princeton University Dept. Mech. & Aero. Engng Rep.* no. 1696.

ROSEN, R., ROSHKO, A. & PARISH, D. L. 1980 A two-layer calculation for the initial interaction region of an unseparated supersonic turbulent boundary layer with a ramp. *AIAA paper* 80–0135.

ROSHKO, A. & THOMKE, G. J. 1969 Supersonic turbulent boundary-layer interaction with a compression corner at very high Reynolds number. *Proc. ARL Symp. on Viscous Interaction Phenomena in Supersonic and Hypersonic Flow*, pp. 109–138. Ohio: University of Dayton Press.

SANDBORN, V. A. 1974 A review of turbulence measurements in compressible flow. *NASA* TMX-62337.

SETTLES, G. S., FITZPATRICK, T. J. & BOGDONOFF, S. M. 1979 Detailed study of attached and separated compression corner flowfields in high Reynolds number supersonic flow. *AIAA J.* **17**, 579–585.

SHIH, T.-H. & LUMLEY, J. L. 1987 Modelling of pressure correlation terms in Reynolds-stress and scalar flux equations. *J. Fluid Mech.* (submitted).

SMITS, A. J., EATON, J. A. & BRADSHAW, P. 1979 The response of a turbulent boundary layer to lateral divergence. *J. Fluid Mech.* **94**, 243–268.

SMITS, A. J. & JOUBERT, P. N. 1982 Turbulent boundary layers on bodies of revolution. *J. Ship Res.* **26**, 135–147.

SMITS, A. J. & MUCK, K. C. 1984 Constant-temperature hot-wire anemometer practice in supersonic flows. Part 2. The inclined wire. *Expts in Fluids* **2**, 33–41.

SMITS, A. J., MUCK, K. C. & HAYAKAWA, K. 1983 Constant-temperature hot-wire anemometer practice in supersonic flows. Part 1. The normal wire. *Expts in Fluids* **1**, 83–92.

SMITS, A. J. & MUCK, K. C. 1987 Experimental study of three shock-wave/turbulent boundary-layer interactions. *J. Fluid Mech.* (to appear).

SMITS, A. J. & WOOD, D. H. 1985 The response of turbulent boundary layers to sudden perturbations. *Ann. Rev. Fluid Mech.* **17**, 321–358.

SMITS, A. J., YOUNG, S. T. B. & BRADSHAW, P. 1979 The effect of short regions of high surface curvature on turbulent boundary layers. *J. Fluid Mech.* **94**, 209–242.

SO, R. M. C. & MELLOR, G. L. 1972 An experimental investigation of turbulent boundary layers along curved surfaces. *NASA* CR-1940.

STUREK, W. B. & DANBERG, J. E. 1972*a* Supersonic turbulent boundary layer in adverse pressure gradient. Part 1. The experiment. *AIAA J.* **10**, 475–480.

STUREK, W. B. & DANBERG, J. E. 1972*b* Supersonic turbulent boundary layer in adverse pressure gradient. Part 2. Data analysis. *AIAA J.* **10**, 630–635.

TAYLOR, M. W. 1984 A supersonic turbulent boundary layer on concavely curved surfaces. M.Sc. thesis, Princeton University. (available as *Dept. Mech. Aerosp. Engng Rept.* 1684).

THOMANN, H. 1968 Effect of streamwise wall curvature on heat transfer in a turbulent boundary layer. *J. Fluid Mech.* **33**, 283–292.

TOWNSEND, A. A. 1976 *The Structure of Turbulent Shear Flow*, 2nd edn., 429 pp. Cambridge University Press.

VAN DRIEST, E. R. 1951 Turbulent boundary layer in compressible fluids. *J. Aero. Sci.* **18**, 145–160.

WALTRUP, P. J. & SCHETZ, J. A. 1973 Supersonic turbulent boundary layer subjected to adverse pressure gradients. *AIAA J.* **11**, 50–58.

WYNGAARD, J. C. 1968 Measurements of small-scale turbulence structure with hot-wires. *J. Phys.* E: *Sci. Instrum.* **1**, 1105.